

LETTER TO THE EDITOR

The $^{35}\text{Cl}/^{37}\text{Cl}$ isotopic ratio in dense molecular clouds: HIFI observations of hydrogen chloride towards W3 A[★]

J. Cernicharo¹, J. R. Goicoechea¹, F. Daniel¹, M. Agúndez^{1,2}, E. Caux³, T. de Graauw⁴, A. De Jonge⁵, D. Kester⁵, H. G. Leduc⁶, E. Steinmetz⁷, J. Stutzki⁸, and J. S. Ward⁹

(Affiliations are available in the online edition)

Received 31 March 2010 / Accepted 12 May 2010

ABSTRACT

We report on the detection with the HIFI instrument on board the *Herschel* satellite of the two hydrogen chloride isotopologues, H^{35}Cl and H^{37}Cl , towards the massive star-forming region W3 A. The $J = 1-0$ line of both species was observed with receiver *Ib* of the HIFI instrument at ~ 625.9 and ~ 624.9 GHz. The different hyperfine components were resolved. The observations were modeled with a non-local, non-LTE radiative transfer model that includes hyperfine line overlap and radiative pumping by dust. Both effects are found to play an important role in the emerging intensity from the different hyperfine components. The inferred H^{35}Cl column density (a few times $\sim 10^{14} \text{ cm}^{-2}$), and fractional abundance relative to H nuclei ($\sim 7.5 \times 10^{-10}$), supports an upper limit to the gas phase chlorine depletion of ≈ 200 . Our best-fit model estimate of the $\text{H}^{35}\text{Cl}/\text{H}^{37}\text{Cl}$ abundance ratio is $\approx 2.1 \pm 0.5$, slightly lower, but still compatible with the solar isotopic abundance ratio (≈ 3.1). Since both species were observed simultaneously, this is the first accurate estimation of the $^{35}\text{Cl}/^{37}\text{Cl}$ isotopic ratio in molecular clouds. Our models indicate that even for large line opacities and possible hyperfine intensity anomalies, the H^{35}Cl and H^{37}Cl $J = 1-0$ integrated line-intensity ratio provides a good estimate of the $^{35}\text{Cl}/^{37}\text{Cl}$ isotopic abundance ratio.

Key words. astrochemistry – ISM: clouds – ISM: molecules – ISM: individual objects: W3 – radiative transfer – radio lines: ISM

1. Introduction

Chlorine has two stable isotopes (^{35}Cl and ^{37}Cl) and an ionization potential of 12.97 eV (i.e., slightly below that of hydrogen). Hence, it can be ionized by UV photons (912–956 Å) in diffuse clouds and in the edges of photon-dissociation regions (PDRs). Once ionized, Cl^+ reacts with molecular hydrogen exothermically to form HCl^+ , a process that initiates the chemical reactions of chlorine. In cloud interiors, HCl^+ can be formed by reactions starting with neutral Cl and H_3^+ . The chemistry of chlorine in interstellar clouds has been the subject of various works (see Neufeld & Wolfire 2009). These studies predict that hydrogen chloride (HCl) is the most abundant Cl-bearing molecule in dense clouds.

The HCl hyperfine lines (see Sect. 3.2) can be resolved in interstellar sources only with heterodyne receivers equipped with high spectral resolution spectrometers. The HCl $J = 1-0$ line at ~ 625.9 GHz was first detected with the Kuiper Airborne Observatory towards Orion (Blake et al. 1985) and followed by detections in Sgr B2 (Zmuidzinas et al. 1995), several positions in OMC-1 (Schilke et al. 1995), and in Mon R2 using the Caltech Submillimeter Observatory with good atmospheric transparency (Salez et al. 1996; SFL96 hereafter). The inferred HCl column densities are in the range 10^{13} – 10^{14} cm^{-2} . SFL96 also presented the first detection of H^{37}Cl towards Orion. Since the chemical reactions involving HCl are relatively well

understood (see Sect. 3.2), the $\text{H}^{35}\text{Cl}/\text{H}^{37}\text{Cl}$ abundance ratio should provide a good measure of the $^{35}\text{Cl}/^{37}\text{Cl}$ isotopic ratio. Both ^{35}Cl and ^{37}Cl nuclei are believed to form in the last burning stages of massive stars ($> 10 M_{\odot}$) and by means of “explosive nucleosynthesis” during supernovae detonation (e.g., Woosley & Weaver 1995). Therefore, observations of H^{35}Cl and H^{37}Cl , and accurate measurements of the $^{35}\text{Cl}/^{37}\text{Cl}$ ratio in different environments, can provide some insight into the chemical evolution of both isotopes, thus into Galactic chemical evolution. The species HCl was also detected recently towards the carbon-rich evolved star IRC+10216 by Cernicharo et al. (2010).

Using HIFI, the Heterodyne Instrument for the Far-Infrared (de Graauw et al. 2010), on board the *Herschel* Space Observatory (Pilbratt et al. 2010), we present in this Letter the detection of the $J = 1-0$ rotational transition of H^{35}Cl and H^{37}Cl towards the massive star-forming region W3. The broad frequency coverage of HIFI allows us to observe both isotopologues of HCl with the same relative calibration in a wide variety of astronomical environments. Here we present the first accurate determination of the $^{35}\text{Cl}/^{37}\text{Cl}$ isotopic ratio by a detailed model of the excitation of the hyperfine levels developed using a non-local radiative transfer code. The effect of line overlaps between the hyperfine components, and radiative pumping by dust photons are discussed and modeled in detail.

2. Observations and data reduction

All spectra presented here were taken during the performance verification (PV) phase of HIFI (de Graauw et al. 2010). Both

[★] *Herschel* is an ESA space observatory with science instruments provided by European-led Principal Investigator consortia and with important participation from NASA.

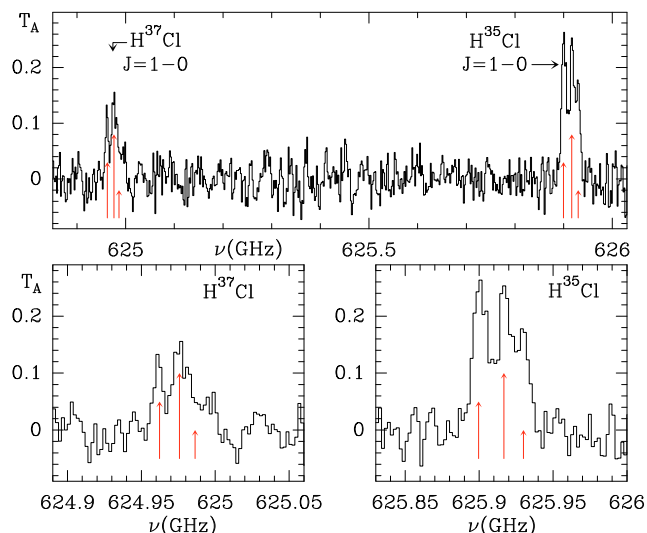


Fig. 1. Detection of H^{35}Cl and H^{37}Cl $J = 1-0$ lines towards W3 A HII region. Arrows show the relative line strength of each HFS component. The length of the arrows are proportional to the expected intensities in the LTE optically thin limit. Both lines were observed simultaneously in a line survey of band 1b of HIFI, hence, have the same calibration accuracy. Spectral resolution was smoothed to 2 MHz ($\approx 1 \text{ km s}^{-1}$).

H^{35}Cl and H^{37}Cl $J = 1-0$ lines were observed in the *Band 1b* receiver using the wide band spectrometer (WBS), which provides $\sim 4 \text{ GHz}$ of bandwidth and $\sim 1.1 \text{ MHz}$ of channel spectral resolution (or a velocity resolution of $\sim 0.5 \text{ km s}^{-1}$ at $\sim 626 \text{ GHz}$). The telescope, which has a half-power beam-width (HPBW) of $\sim 35''$ at $\sim 626 \text{ GHz}$, was centered on $\alpha_{2000} = 02^{\text{h}}25^{\text{m}}43.51^{\text{s}}$, $\delta_{2000} = 62^{\circ}06'13''$ (a position close to W3 A IRS 2 and 2a). A complete spectral scan of the *Band 1b* was taken at this position during PV phase and several lines from different molecules have been identified so far. The horizontal (H) and vertical (V) polarization receivers were averaged after rescaling the V one using the HCO^+ $J = 7-6$ line intensity at 624.21 GHz , i.e., close to that of HCl isotopologues. The data were first processed with HIPE software (Ott et al. 2010), and then exported to CLASS where standard data reduction routines were carried out. We checked that the target lines are not contaminated by lines from the other side band using the different frequency settings. The rms noise at $\sim 626 \text{ GHz}$ is $\sim 30 \text{ mK}$ (antenna temperature) per 0.5 km s^{-1} resolution channel. Hence, the H^{35}Cl and H^{37}Cl $J = 1-0$ lines are detected at 10σ and 6σ levels, respectively and with the same relative calibration. At this level of sensitivity, only the most abundant species are detected. In particular, we detected 20 lines in the entire band 1b above 3σ . The brightest is the CO $J = 5-4$ line, followed by the ground-state line of ortho- H_2O and a few lines from formaldehyde, methanol, HCO^+ , and HCN. Hence, we are confident that the observed HCl line profiles are not blended with other spectral features. By examining our own and public spectral catalogs (Muller et al. 2001, 2005; Pickett et al. 1998), we also checked that lines in the signal band from other molecules do not blend with the hyperfine components of both HCl isotopologues.

The total integration time was 2 min. Figures 1 and 2 show the resulting line profiles (data smoothed to a spectral resolution of $\approx 1 \text{ km s}^{-1}$). To compare with our models, the following expression for the main beam efficiency was adopted, $\eta_{\text{mb}} = 0.72 \exp(-(\nu/6)^2) \times 0.96$, where ν is the frequency in THz, 0.72 is η_{mb} for the telescope in the limit of 0 frequency, and the factor

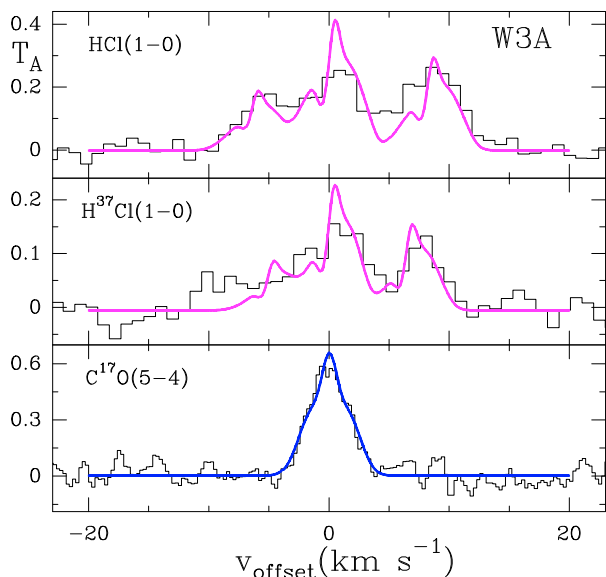


Fig. 2. H^{35}Cl , H^{37}Cl $J = 1-0$, and C^{17}O $J = 5-4$ lines observed with HIFI towards W3 A. Continuous curves show closest fitting radiative-transfer model line profiles (see text). The spectral resolution is $\approx 1 \text{ km s}^{-1}$.

0.96 is the assumed forward efficiency of the telescope (Olberg priv. comm.).

3. Results

In terms of spectroscopy, the $I = 3/2$ nuclear spin of ^{35}Cl and of ^{37}Cl splits the pure rotational transitions of H^{35}Cl and H^{37}Cl into several hyperfine structure (HFS) components (see e.g., Cazoli & Puzzarini 2004 and references therein). These hyperfine components are indicated as vertical arrows in Fig. 1. In the optically thin limit, these components follow a 2:3:1 intensity ratio (from the lowest to the highest frequency hyperfine component). It is clear from Fig. 1 that the observed ratios are close to 1:1:1 for the three hyperfine components of H^{35}Cl . These ratios indicate that the H^{35}Cl hyperfine components are affected substantially by opacity. Even for H^{37}Cl , the observed hyperfine line intensities (1:1:2) do not follow the expected ratios in an optically thin case.

The intensity peak ratio of the strongest H^{35}Cl and H^{37}Cl HFS components is ≈ 1.5 and the integrated intensity ratio is $\approx 2 \pm 0.2$. These values are lower than the solar $^{35}\text{Cl}/^{37}\text{Cl}$ abundance ratio, ~ 3.1 (Anders & Grevesse 1989), which suggests that optical depth effects could influence the observed HFS line intensity ratios (or that the $\text{H}^{35}\text{Cl}/\text{H}^{37}\text{Cl}$ abundance ratio is lower than the solar value). For completeness, Fig. 2 compares the detected HCl lines with the C^{17}O $J = 5-4$ at 561.712 GHz also observed with HIFI. The detection of C^{17}O , HCO^+ and HCN mid- J lines confirms the presence of warm and dense molecular gas towards the observed position.

3.1. HCl excitation and $^{35}\text{Cl}/^{37}\text{Cl}$ abundance ratio

The star-forming region W3 is located in the Perseus arm at a distance of 2.3 kpc and contains several young massive stars that ionize a natal molecular cloud creating HII regions. In particular, the near-IR sources IRS 2 and IRS 2a (OB stars) are believed to be the ionizing sources of the W3 A HII region (Tieftrunk et al. 1995 and references therein). These sources are also the origin of molecular outflows and are X-rays emitters (Hofner et al. 2002).

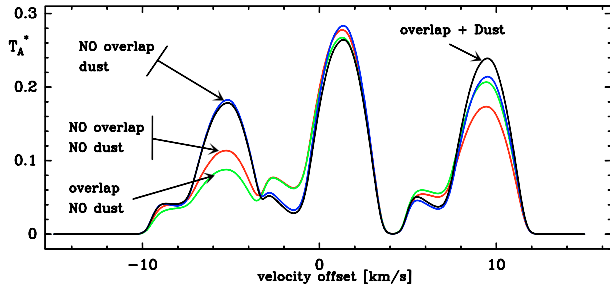


Fig. 3. Results from non-local, non-LTE radiative transfer calculations for the H^{35}Cl $J = 1-0$ HFS components. The different curves show the effects of including line overlap and radiative pumping from dust photons in the emerging line intensities and relative HFS line ratios.

To estimate the $\text{H}^{35}\text{Cl}/\text{H}^{37}\text{Cl}$ abundance ratio and analyze all possible effects affecting the emerging line profiles, we modeled the observed HCl and C^{17}O lines with our non-local and non-LTE radiative transfer codes (González-Alfonso & Cernicharo 1993, 1997; Goicoechea et al. 2006; Daniel & Cernicharo 2008). To take into account the blending of the HCl $J = 1-0$ hyperfine components (i.e., to determine the opacity at each frequency when several lines overlap), we used the modelling approach presented in Daniel & Cernicharo (2008) to interpret the HFS line emission from N_2H^+ , HCN, and HNC. Rate coefficients for the collisional excitation of HCl by He are taken from Neufeld & Green (1994), who also estimated the contribution to each specific hyperfine level. Like other light hydrides that HIFI will observe, HCl has a large rotational constant (10.4 cm^{-1}), thus HCl rotational transitions have high spontaneous radiative rates. The HCl critical densities are very high, $n_{\text{cr}}(J = 1-0) \approx 7 \times 10^7 \text{ cm}^{-3}$, and only when $n(\text{H}_2) \gtrsim n_{\text{cr}}$ does collisional excitation dominate. This high value suggests that HCl line emission arises in dense molecular gas. Radiative pumping by dust photons may also be very important in determining the HCl level populations (see also SFL96) because of the increase in grain emissivity and dust opacity in the far-IR and submillimeter domains (Cernicharo et al. 2006a,b). Model predictions shown in Fig. 3 demonstrate that the inclusion of line overlap, dust pumping, and both effects together, modifies the relative intensity of each HFS component. We note in particular how the $J = 1-0F = 1/2-1/2$ line (the HFS component with the weakest line strength and opacity) is enhanced with respect to the other components when radiative pumping is included.

To reproduce the observed H^{35}Cl and H^{37}Cl line profiles and relative intensities, we assumed uniform physical conditions ($n_{\text{H}} \approx 10^6 \text{ cm}^{-3}$ and $T_{\text{k}} \approx 100 \text{ K}$; taken from Helmich et al. 1994; Tieftrunk et al. 1995) and that the H^{35}Cl and H^{37}Cl abundances are free parameters. The C^{17}O line was also analyzed with the same parameters to verify the model consistency. In particular, the C^{17}O $J = 5-4$ line was found to be optically thin ($\tau \approx 0.1$), which allowed us to constrain the line-of-sight column density of material and also the line velocity dispersion ($\sigma \approx 1.3 \text{ km s}^{-1}$). Gas and dust were assumed to coexist and be thermally coupled ($T_{\text{k}} = T_{\text{d}}$).

To reproduce the observed HCl line peak positions and their relative strengths, best fit solutions were obtained for an expanding shell of gas. The adopted velocity gradient (from 2.5 km s^{-1} at the center to 0.5 km s^{-1} at the edge) is consistent with the CO molecular outflows seen in the region (e.g., Hasegawa et al. 1994). Optimal results were obtained for a H^{35}Cl column density of a few times 10^{14} cm^{-2} (or an abundance of $\sim 7.5 \times 10^{-10}$

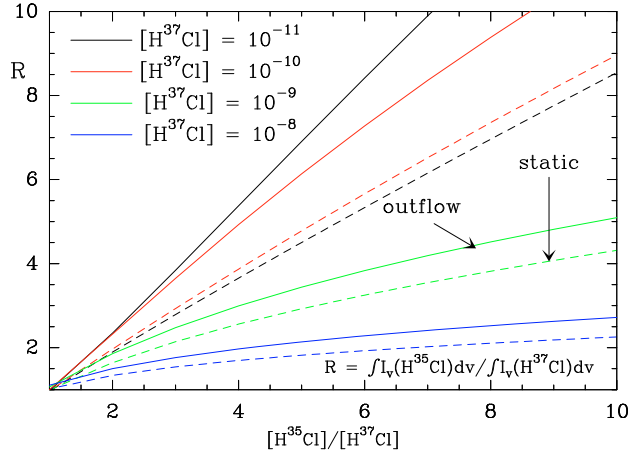


Fig. 4. Modeled HCl and H^{37}Cl $J = 1-0$ integrated line intensity ratio (R) as a function of the assumed isotopic abundance ratio (see text). HCl abundances, indicated at the top left, are relative to H nuclei. Continuous lines correspond to models with a velocity gradient. Dashed lines correspond to a static model.

relative to total H). The inclusion of radiative pumping from dust (and line overlap to a lesser extent) allowed one to more accurately reproduce the observed HFS relative line intensities. Assuming that H^{35}Cl and C^{17}O arise from the same regions, we inferred a column density ratio of $N(\text{H}^{35}\text{Cl}) \approx N(\text{C}^{17}\text{O})/20$, by using the CO abundance determined for the region ($\sim 4 \times 10^{-5}$ per H nucleus; Tielens et al. 1991) and assume a standard $^{16}\text{O}/^{17}\text{O}$ isotopic ratio of 2600. Optimal fits were obtained by using an automatic χ^2 procedure and are shown in Fig. 2. The $\text{H}^{35}\text{Cl}/\text{H}^{37}\text{Cl}$ abundance ratio in the models is ~ 2.1 (with a confidence interval within 1.6–3.1). Since H^{35}Cl lines are moderately optically thick ($\tau \sim 12, 8, 4$ for each HFS component), one does not expect the observed $\text{H}^{35}\text{Cl}/\text{H}^{37}\text{Cl}$ line intensity ratio to provide a direct measure of the $\text{H}^{35}\text{Cl}/\text{H}^{37}\text{Cl}$ abundance ratio. However, HCl critical densities are much higher than the gas density in most ISM clouds, and therefore the excitation temperature of the different HFS components remain proportional to the HCl column density, even for optically thick lines. To conclude whether or not the line integrated intensity ratio is a good measure of the isotopic abundance ratio, Fig. 4 shows the modeled integrated intensity ratio as a function of the $\text{H}^{35}\text{Cl}/\text{H}^{37}\text{Cl}$ abundance ratio. Although the hyperfine components are optically thick in most models, the integrated line intensity ratio is proportional to the isotopic ratio for HCl abundances below 10^{-9} . In Fig. 4, we also show the results for a static cloud. In this case, the opacities are larger but the integrated intensity ratio still provides a reliable measurement of the isotopic abundance ratio for HCl abundances below 10^{-10} .

3.2. Chlorine chemistry in W3A HII region

In the UV-illuminated gas, the chlorine chemistry involves the reaction of Cl^+ with molecular hydrogen to form HCl^+ , which then reacts with H_2 to produce H_2Cl^+ . If the abundance of electrons is high, dissociative recombination of H_2Cl^+ leads to the formation of HCl with a typically assumed branching ratio of $\sim 10\%$. In cloud interiors, atomic chlorine is mostly neutral, not ionized, so that the reaction of Cl and H_3^+ drives the formation of H_2Cl^+ , which then reacts with CO and H_2O leading to the formation of HCl. An alternative direct route to HCl in either hot gas or regions where vibrationally excited H_2 is abundant (e.g., Agúndez et al. 2010) is the $\text{Cl} + \text{H}_2 \rightarrow \text{HCl} + \text{H}$ reaction,

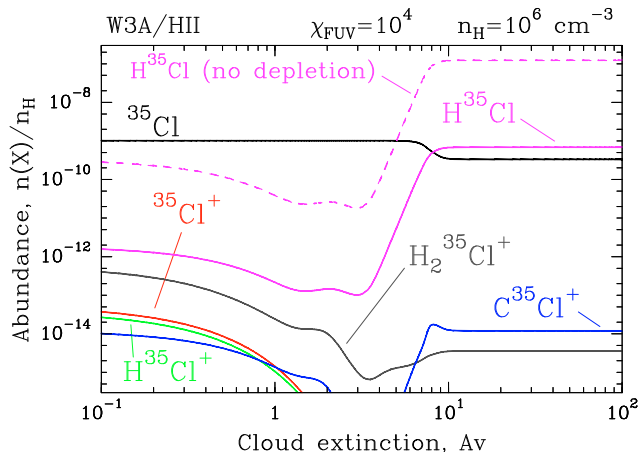


Fig. 5. Cloud-depth dependent photochemical models adapted to W3 A physical conditions. The gas density ($n_{\text{H}} = 10^6 \text{ cm}^{-3}$) and temperature ($T_k = 100 \text{ K}$) are kept constant. The UV radiation field is $\chi = 10^4$ and the ionization rate due to cosmic rays is $\zeta(\text{H}) = 2.5 \times 10^{-17} \text{ s}^{-1}$. The predicted abundance of several Cl-bearing species are shown. A chlorine gas-phase abundance of 1×10^{-9} is used. The dashed line shows the expected HCl abundance with an undepleted abundance of $[\text{Cl}] = 1.8 \times 10^{-7}$.

which possesses an energy barrier of $\sim 0.2 \text{ eV}$ (Dobis & Benson 2002). The destruction of HCl is dominated both by photoionization and photodissociation and by reactions with C^+ and H_3^+ (the latter in the UV shielded gas). Previous observational studies of HCl suggest that there has been a depletion of gas-phase chlorine in dense molecular clouds of a factor of >100 (SFL96) relative to the elemental chlorine abundance observed in diffuse clouds ($[\text{Cl}] \approx 1.8 \times 10^{-7}$; Savage & Sembach 1996, Sonnentrucker et al. 2006 and references therein). To follow the HCl chemistry in the particular environment of W3 A HII region and estimate the Cl depletion we modeled the Cl-photochemistry using the Meudon PDR code (Le Petit et al. 2006; Goicoechea & Le Bourlot 2007). The reaction network for Cl-bearing molecules includes the updated rates of Neufeld & Wolfire (2009). We note that the X-ray luminosity reported in the region ($L_{\text{X}} \sim 5 \times 10^{31} \text{ erg s}^{-1}$; Hofner et al. 2002) is insufficient for a “XDR-” rather than a “PDR-dominated” environment. However, in cloud interiors X-ray photons may play an important role in the Cl-chemistry.

Figure 5 shows the output of a model adapted to the physical conditions in W3 A. The UV radiation field produced this volume by the OB stars in the region is simulated by an enhancement of 10^4 times the mean interstellar radiation field (in Draine units). To reproduce the inferred H^{35}Cl abundance ($\sim 7.5 \times 10^{-10}$), a gas-phase chlorine depletion of ≤ 200 is needed, HCl accounting for $\approx 70\%$ of the Cl nuclei in the gas phase. This conclusion is reached assuming that the observed HCl arises in regions of large H_2 column density ($A_{\text{V}} \geq 100$; see Sect. 3.1), which is consistent with the submm continuum maps of the region (Jaffe et al. 1983). If the observed HCl arises in regions of lower extinction, the Cl depletion factor will obviously be lower.

4. Conclusions

We have presented the first detection of H^{35}Cl and H^{37}Cl towards the W3 A HII region. The inferred H^{35}Cl column density (a few times $\sim 10^{14} \text{ cm}^{-2}$) and fractional abundance ($\sim 7.5 \times 10^{-10}$ per H nucleus) provide an upper limit to the gas phase chlorine

depletion of ≈ 200 . This value is lower than that observed towards Orion hot core, but similar to that inferred towards Mon R2 (SFL96). Radiative transfer models including HFS line overlap and pumping by dust photons have been used to interpret the observations. The best-fit model provides a $\text{H}^{35}\text{Cl}/\text{H}^{37}\text{Cl}$ abundance ratio of ≈ 2.1 , which is both lower than the solar value (≈ 3.1) and lower than the previous estimate towards Orion ($\approx 4-6$; SFL96). On the other hand, it is similar to the $[\text{Cl}^{35}]/[\text{Cl}^{37}]$ ratio obtained in the IRC+10216 circumstellar envelope from $[\text{Na}^{35}\text{Cl}]/[\text{Na}^{37}\text{Cl}]$ and $[\text{Al}^{35}\text{Cl}]/[\text{Al}^{37}\text{Cl}]$ measurements (Cernicharo & Guélin 1987; Cernicharo et al. 2000).

Acknowledgements. HIFI has been designed and built by a consortium of institutes and university departments from across Europe, Canada and the United States under the leadership of SRON Netherlands Institute for Space Research, Groningen, The Netherlands and with major contributions from Germany, France and the US. Consortium members are: Canada: CSA, U. Waterloo; France: CESR, LAB, LERMA, IRAM; Germany: KOSMA, MPIfR, MPS; Ireland: NUI Maynooth; Italy: ASI, IFSI-INAF, Osservatorio Astrofisico di Arcetri-INAF; Netherlands: SRON, TUD; Poland: CAMK, CBK; Spain: Observatorio Astronómico Nacional (IGN), Centro de Astrobiología (CSIC-INTA). Sweden: Chalmers University of Technology - MC2, RSS & GARD; Onsala Space Observatory; Swedish National Space Board, Stockholm University - Stockholm Observatory; Switzerland: ETH Zurich, FHNW; USA: Caltech, JPL, NHSC. We thank the Spanish MICINN for funding support through grants AYA2006-14876, AYA2009-07304, and and Consolider project CSD2009-00038. J.R.G. is supported by a Ramón y Cajal research contract from the Spanish MICINN. MA is supported by a Marie Curie Intra-European Individual Fellowship within the EC FP7 under grant agreement no 235753.

References

- Agúndez, M., Goicoechea, J. R., et al. 2010, *ApJ*, 713, 662
 Anders, E., & Grevesse, N. 1989, *GeCoA.*, 53, 197
 Blake, G. A., Keene, J., & Phillips, T. G. 1985, *ApJ*, 295, 501
 Cazoli, G., & Puzzarini, C. 2004, *JMoSp.*, 226, 161
 Cernicharo, J., & Guélin, M. 1987, *A&A*, 183, L10
 Cernicharo, J., Kahane, C., & Guélin, M. 2000, *A&AS*, 142, 181
 Cernicharo, J., Goicoechea, J. R., Pardo, J. R., et al. 2006a, *ApJ*, 642, 940
 Cernicharo, J., Goicoechea, J. R., Daniel, F., et al. 2006b, *ApJ*, 649, L33
 Cernicharo, J., et al. 2010, *A&A*, 518, L136
 Daniel, F., & Cernicharo, J. 2008, *A&A*, 488, 1237
 Dobis, O., & Benson, S. W. 2002, *J. Phys. Chem. A*, 106, 4403
 de Graauw, Th., et al. 2010, *A&A*, 518, L6
 Goicoechea, J. R., Pety, J., Gerin, M., et al. 2006, *A&A*, 456, 565
 Goicoechea, J. R., & Le Bourlot, J. 2007, *A&A*, 467, 1
 González-Alfonso, E., & Cernicharo, J. 1993, *A&A*, 279, 506
 González-Alfonso, E., & Cernicharo, J. 1997, *A&A*, 322, 938
 Hasegawa, T. I., Mitchell, G. F., et al. 1994, *ApJ*, 426, 215
 Helmich, F. P., Jansen, D. J., de Graauw, Th., et al. 1994, *A&A*, 283, 626
 Hofner, P., Delgado, H., Whitney, B., et al. 2002, *ApJ*, 579, L95
 Jaffe, D. T., Hildebrand, R. H., Keene, J., et al. 1983, *ApJ*, 273, L89
 Le Petit, F., Nehmé, C., Le Bourlot, J., & Roueff, E. 2006, *ApJS*, 64, 506
 Muller, H. S. P., Thorwirth, S., Roth, D. A., & Winnewisser, G. 2001, *A&A*, 370, L49
 Muller, H. S. P., Schlder, F., et al. 2005, *J. Mol. Struct.* 742, 215
 Neufeld, D. A., & Green, S. 1994, *ApJ*, 432, 158
 Neufeld, D. A., & Wolfire, M. G. 2009, *ApJ*, 706, 1594
 Ott, S., et al. 2010, in *Astronomical Data analysis Software and Systems XIX*, ed. Y. Mizumoto, K. I. Morita, & M. Ohishi, ASP Conf. Ser.
 Pickett, H. M., Poynter, I. R. L., Cohen, E. A., et al. 1998, *J. Quant. Spectrosc. & Rad. Transfer*, 60, 883
 Pilbratt, G. L., et al. 2010, *A&A*, 518, L1
 Salez, M., Frerking, M. A., & Langer, W. D. 1996, *ApJ*, 467, 708
 Savage, B. D., & Sembach, K. R. 1996, *ARA&A*, 34, 279
 Schilke, P., Phillips, T. G., & Wang, N. 1995, *ApJ*, 441, 334
 Sonnentrucker, P., Friedman, S. D., & York, D. G. 2006, *ApJ*, 650, L115
 Tiefrunk, A. R., Wilson, T. L., Steppe, H., et al. 1995, *A&A*, 303, 901
 Tielens, A. G. G. M., Tokunaga, A. T., Geballe, T. R., & Baas, F. 1991, *ApJ*, 381, 181
 Woosley, S. E., & Weaver, T. A. 1995, *ApJS*, 101, 181
 Zmuidzinas, J., Blake, G. A., Carlstrom, J., et al. 1995, *ApJ*, 447, L125

-
- ¹ Centro de Astrobiología. CSIC-INTA. Carretera de Ajalvir, Km 4, Torrejón de Ardoz. 28850, Madrid, Spain
e-mail: jcernicharo@cab.inta-csic.es
- ² LUTH, Observatoire de Paris-Meudon, 5 Place Jules Janssen, 92190 Meudon, France
- ³ Centre d'Étude Spatiale des Rayonnements, Université de Toulouse [UPS], 31062 Toulouse Cedex 9, France
- ⁴ Atacama Large Millimeter/Submillimeter Array, ALMA Office, Santiago, Chile

- ⁵ SRON Netherlands Institute for Space Research, Landleven 12, 9747 AD Groningen, The Netherlands
- ⁶ Jet Propulsion Laboratory, 4800 Oak Grove Drive, MC 302-231, Pasadena, CA 91109, USA
- ⁷ MPI für Sonnensystemforschung, 37191 Katlenburg-Lindau, Germany
- ⁸ KOSMA, I. Physik. Institut, Universität zu Köln, Germany
- ⁹ With Raytheon Co., Fort Wayne, Indiana, USA, since March of 2009